NIST Advanced Manufacturing Series
NIST AMS 100-56

Powder Spreading Testbed for Studying the Powder Spreading Process in Powder Bed Fusion Machines

Justin Whiting
Eric Whitenton
Aniruddha Das
Vipin Tondare
Jason Fox
Michael McGlauflin
Alkan Donmez
Shawn Moylan

This publication is available free of charge from:
https://doi.org/10.6028/NIST.AMS.100-56

NIST NATIONAL INSTITUTE OF STANDARDS AND TECHNOLOGY
U.S. DEPARTMENT OF COMMERCE

NIST Advanced Manufacturing Series
NIST AMS 100-56

Powder Spreading Testbed for Studying the Powder Spreading Process in Powder Bed Fusion Machines

Justin Whiting
Eric Whitenton
Aniruddha Das
Vipin Tondare
Michael McGlauflin
Alkan Donmez
Shawn Moylan
Intelligent Systems Division
Engineering Laboratory

This publication is available free of charge from:
https://doi.org/10.6028/NIST.AMS.100-56

November 2023

U.S. Department of Commerce
Gina M. Raimondo, Secretary

National Institute of Standards and Technology
Laurie E. Locascio, NIST Director and Under Secretary of Commerce for Standards and Technology

NIST AMS 100-56
November 2023

Disclaimer

Certain commercial equipment, instruments, software, or materials, commercial or non-commercial, are identified in this paper in order to specify the experimental procedure adequately. Such identification does not imply recommendation or endorsement of any product or service by NIST, nor does it imply that the materials or equipment identified are necessarily the best available for the purpose.

NIST Technical Series Policies

Publication History

Approved by the NIST Editorial Review Board on 2023-11-29

How to Cite this NIST Technical Series Publication

Whiting J, Whitenton E, Das A, Tondare V, Mcglauflin M, Donmez A, Moylan S (2023) Powder Spreading Testbed for Studying the Powder Spreading Process in Powder Bed Fusion Machines. (National Institute of Standards and Technology, Gaithersburg, MD), NIST Advanced Manufacturing Series (AMS) NIST AMS 100-56. https://doi.org/10.6028/NIST.AMS.100-56

NIST Author ORCID iDs

Justin Whiting: 0000-0003-0264-1349
Eric Whitenton: 0000-0002-8706-7413
Aniruddha Das: 0000-0002-6451-1657
Vipin Tondare: 0000-0002-0483-1990
Michael McGlauflin: None
Alkan Donmez: 0000-0002-1324-1642
Shawn Moylan: 0000-0003-3927-1118

Contact Information

aniruddha.das@nist.gov

Mailing Address

A115, Sound Building (233), NIST
Gaithersburg, MD, 20878

Abstract

The spreading of powder is an integral part of powder bed fusion-based additive manufacturing technologies; however, due to the complex nature and the number of interactions between particles, studying the powder spreading process is difficult. In order to gain insight into how the metal powder is spread in powder bed fusion machines using a recoater, a spreading testbed is needed, which provides a method for investigating the powder spreading process and characterizing the powder spread layer. The objective of this testbed is to study and establish fundamental relationships between bulk metal powder characteristics and powder spreading performance. Here, fabrication of a powder spreading testbed (PST) is described. The minimum but necessary functionality of the PST is discussed and potential characterization methods for the powder spread layer are proposed. This document serves as a guideline for future enhancements to the present testbed.

Keywords

Laser Powder Bed Fusion, Powder spreading, Powder spreadability, Testbed, Particle tracking, Additive manufacturing.

Table of Contents

1. Introduction **1**
2. Powder Spreading Testbed at NIST **6**
2.1. The appearance and dimensions of the PST. 7
2.2. Vibration analysis of the PST 10
2.3. Powder heap creation methods 11
2.4. Powder spreading method 12
2.5. Cross-sectional imaging for particle tracking 13
3. An initial result and a brief methodology of particle tracking **16**
4. Characterization of spread powder layer **19**
4.1. Particle Size Distribution (PSD) 19
4.2 Spread layer height 20
4.3 Powder layer density 21
5. Environmental chamber 22
6. Conclusion **22**
References **23**
Appendix **26**

List of Tables

Table 1. Summary of variables that can affect powder spreading. 3
Table 2. Magnifications achievable with the commonly used lens systems. 14

List of Figures

Fig. 1. Collected from the work of Oropeza et al.[28]. A powder spreading testbed: (a) computer model showcasing major components with the roller as the powder spreading mechanism; (b) fabricated powder spreading testbed; (c) sectional side-view of the testbed highlighting moving components and motion trajectories ; (d) images from the powder spreading experiment using stainless steel 316L 15 μm–45 μm powder and 250 μm layer height (Permission to reproduce these images was obtained from the authors and the publisher). 5
Fig. 2. (a) The PST is viewed from a side including labels for relevant components, the baseplate is seen in front and the XPS Q8 controller is seen at the rear and (b) a front view of the PST. 8
Fig. 3. A triaxial accelerometer is mounted on the recoater bridge to measure vibration. ... 10
Fig. 4. (a) The plastic stencil placed with powder poured into it and (b) the heap of powder after removing the stencil. The blue light seen in the images are not a part of the PST but results from the handheld camera used for taking the photographs. 11

Fig. 5. (a) The cylinder is filled with powder, lifted, and placed on the PST, and (b) the heap of powder is created by turning the cylinder using the white knob at the end. 12
Fig. 6. The Photron NOVA high-speed camera positioned to look into the PST for videography 14
Fig. 7. Still image of recoater blade spreading stainless steel powder captured using the high-speed camera set up. The field of view measures 2.71 mm x 2.33 mm. 15
Fig. 8. Still imagery extracted from high-speed videography (total 116 ms long) of powder spreading: (a) heap advancing before spreading (after 43 ms), (b) during spreading (after 78 ms), and (c) after the front of the blade has passed (after 116 ms). The field of view measures 2.71 mm x 2.33 mm and the scaling is 2.71 μm/pixel. 16
Fig. 9. Plot of particle track data using random colors 17
Fig. 10. Plot of the vector field with colors indicating velocity relative to the stationary camera. Since the baseplate of the PST is also stationary, this plot is especially informative near the baseplate, since it may indicate what frictional forces are likely between the particles and the baseplate 18
Fig. 11. Plot of the vector field with colors indicating velocity relative to the blade. This plot is especially informative near the blade, since it may indicate what frictional forces are likely between the particles and the blade 18
Fig. 12. (a) Image showing the LK G32 laser point scanner attached to the recoater arm of the PST, the black lens of the Photron NOVA high speed video camera is visible in the background, (b) plot of height data over the entire span of spread powder (set 2 indicates the second scan) and (c) zoomed-in view of height data at 50-51 mm of the same powder spread. 21

1. Introduction

As the additive manufacturing (AM) field continues to grow, the need to further our understanding of each stage of the process does as well. In the powder bed fusion process (PBF), thin layers of granular material (e.g., metal or polymer powder) are deposited so that they can be joined together with an energy source, often a laser or electron beam. The high-resolution, programmable area of exposure and layer-wise nature of this fusion allows complex geometries to be created. In the PBF process, the material is deposited using a recoating mechanism to deposit layers of powder, most commonly at thicknesses on the order of 20 μm to 100 μm [1]. The recoating mechanism is often a rigid blade of various materials, but a flexible material or cylindrical 'roller' is also found in commercial systems, as is the case for polymer PBF. There are also contactless recoating processes that utilize electrostatic or gravitational forces for powder deposition [2, 3]. The action of recoating may also involve control over the amount of pressure exerted by a spreader over the spread powder layer [4]. Theoretically, it is also possible to introduce or control the vibration of the spreader during powder spreading [5].

The testbed described in this document focuses on a metal powder spreading process using a rigid recoater blade, in a laser powder bed fusion (LPBF) machine. While much of the research in the LPBF AM field is rightfully focused on the complex interaction between the energy source and the powder bed (i.e., melt pool), much less focus is placed on the deposition of the feedstock powder. Variability has been documented in the mechanical properties of final PBF parts including hardness, tensile strength, and ductility [6, 7]. Though various hypotheses have been made regarding the origin, the contribution of the powder layer characteristics to this variability cannot be ruled out and deserves investigation. For example, as shown by Slotwinski et al. and Whiting et al., there seems to be an inherent variation in the particle size distribution (PSD) along the spreading direction [8, 9].

The characteristics of a spread layer will affect the melting and solidification processes and ultimately the final part properties. The density, height, and PSD of a spread layer of powder may be location dependent. To understand how a layer of powder is spread, the powder must be evaluated in a similarly dynamic state. Intrinsic properties of the feedstock material undoubtedly play a role in determining this dynamic performance, but it is difficult, if not impossible, to predict the quality of a spread layer considering only the powder's intrinsic properties. Because LPBF precursor materials are on the order of tens of micrometers in size, characterization of the dynamic performance can be challenging. They are easily disturbed and subject to forces from static charging, Van der Waals, and liquid bridging [10]. Much of the existing research uses benchtop tools to evaluate the bulk flow (dynamic properties) of the metal powders. Both conventional (e.g., angle of repose, funnel flowmeters) and novel (e.g., rotating drum or blade rheometer) methods have been used to quantify these properties of metal AM powders [11, 12]. Two common standard test methods for metal powder characterization are ASTM B213-17 and ASTM B527-22 [13, 14]. The former describes the method for evaluating the flow rate of a powder using the Hall Flowmeter (i.e., a well-defined funnel geometry). The latter describes a method for measuring the tapped density of a powder, which is the maximum density of a powder after being subjected to repeated drops. In a blade rheometer, the powder is placed

inside a vessel where a blade is driven through the powder while the normal force (either measured below the vessel or on the blade's shaft) and the torque (measured via the load on the motor) are measured. Other methods, like the rotating drum and angle of repose, use a visual inspection to judge the powder's behavior. The rotating drum method allows the profile of a volume of powder contained in a cylinder with transparent end faces to be visualized while the drum rotates. The method initially developed by Kaye et al. has since been commercialized with companies using various techniques to extract metric(s) from the process (e.g., avalanche angle and rate, geometrical descriptors of the surface) [15, 16].

These *ex-situ* characterization methods subject the powder to various stresses and provide metric(s) to quantify the powder's performance. There is a question in terms of the relevance of these methods: How can the metrics be used if their relationship to LPBF or, more simply, the act of spreading powder is not understood? The metrics obtained are a function not only of the powder's intrinsic properties but also the conditions of the stress and environmental conditions. If the measurand (e.g., force, torque, and profile of powder) is acquired in a stress condition different than that of a spreading process, the data cannot directly be used to deduce the spreading performance of a metal powder in the LPBF process. While a relationship likely exists between the measurand and the spreading performance based on the powder's intrinsic properties, until that relationship is well understood, the spreading performance cannot be inferred. We designed a powder spreading testbed (PST) as summarized in this document to help gain the knowledge needed to develop this relationship. **Table 1** shows a summary of variables that can affect powder spreading.

Table 1. Summary of variables that can affect powder spreading.

Powder related	Environment related	Solid edges encountered	Surface related	Machine or spreading-related
Powder material	Gas flow or low pressure such as in denudation	Part geometry and orientation	Surface characteristics of the solidified layer of the part being printed	Recoater type or geometry
Powder history (changes to density, segregation)	Humidity (moisture content of ambient)	Position and orientation of powder solid transitions (solid edges) in the previous layer	Surface characteristics of the substrate	Recoater velocity or recoating action (pressure or movement control)
Moisture content of the powder	Electrostatic charge and triboelectric properties of material/recoating mechanism/build substrate			Recoater material
Van der Walls forces				Layer height
Powder morphology				Charge factor (i.e., heap size)

Since granular flow can be modeled with the discrete element method (DEM), most research articles have used this tool for powder spreading simulation. Various efforts using DEM to model the spreading of powders in PBF have been made, but they seldom use metrics of the actual spreading process to calibrate or validate the model [13, 14, 17–20]. Yao et al. evaluated ideal spreading parameters via DEM simulation of SS 316L powder with a blade-type spreader, mimicking conditions in LPBF equipment. Using DEM simulations to maximize the packing density of the spread layer, the optimal values for the recoater blade angle, particle diameter, and recoater blade speed were evaluated [21]. The results of these simulations can be verified using the PST. Zhang et al. tracked particle trajectory and displacement parameters along with the distribution of forces to compare (a) Blade and (b) Roller-based spreading using DEM simulation [22]. These two methods were also compared by Haeri et al. using DEM [23]. Both works indicated that the roller applies higher contact pressure compared to blade-based spreading. Haeri et al. also worked on the influence of particle alignment and shape segregation with recoating speed using DEM. Further comparisons involving the simulation of spreading outcomes with various blade shapes and a roller-based spreader were conducted by Wang et al. [24]. Differences in size segregation are observed with changes in spreader shape. Modifications of existing techniques to spread powder have also been suggested for improvements in bed quality. For example, Ganesan et al. conceptualized and simulated a technique for lateral powder compaction after blade-based powder spreading to improve densification of the spread layer

[25]. Powder flow simulations in the case of powder spreading have also been studied in detail by Nan et al. using DEM [26]. It was observed that the mass flow rate at the recoater-baseplate or recoater-powder bed became constant after a limiting recoater velocity (namely, critical velocity or V_c). This indicates that the bed quality remains unchanged beyond critical velocity.

In efforts to measure spreading performance more directly, several recent studies describe the development of powder spreading testbeds. Hulme et al. used a commercially available thin film applicator, used in the paint and food industries, with an adjustable blade height as a spreading platform [27]. A custom-designed powder dispenser was developed to repeatably generate the initial heap geometry before spreading. By capturing images of the spread powder area on the platform and through the resulting image analysis, they defined three parameters as metrics for spreadability: actual area of coverage, the convex hull of the spread area, and the bounding box of the spread area. Using these metrics, they compared three different powder samples spread using four different recoater speeds. They concluded that all three metrics have to be used to fully describe the powder flow characteristics.

Oropeza et al. describe the design, fabrication, and qualification of a modular testbed for multi-layer powder spreading as shown in **Fig. 1** [28]. This testbed replicates the operating conditions of commercial AM machines with full control over motion parameters to investigate the optimization of spreading parameters. Uniformity of the spread powder layer is assessed, using an imaging setup over the build platform (digital camera with zoom lens) with coaxial and lateral lighting, as the differences in brightness of the spread area. They indicated their future plans were to incorporate appropriate powder bed density and surface roughness measurements into this testbed.

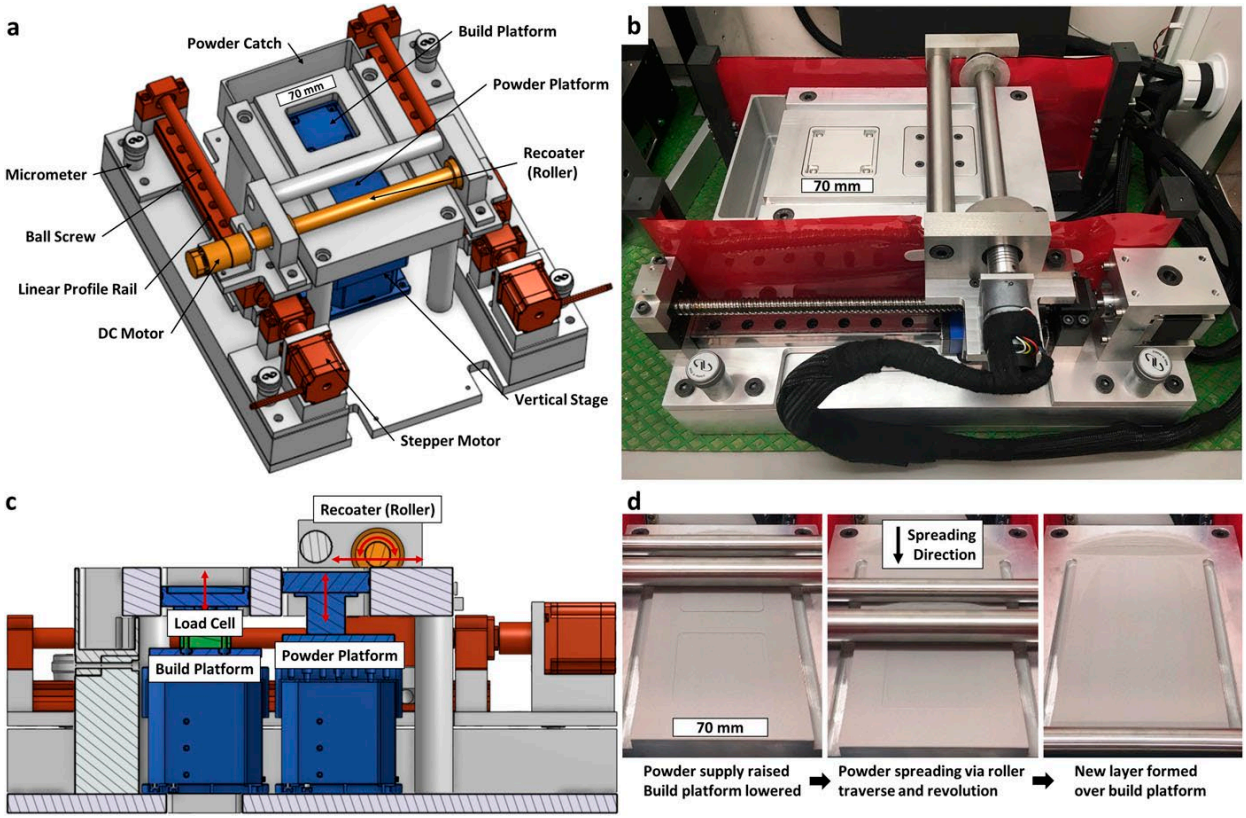

Fig. 1. Collected from the work of Oropeza et al.[28]. A powder spreading testbed: (a) computer model showcasing major components with the roller as the powder spreading mechanism; (b) fabricated powder spreading testbed; (c) sectional side-view of the testbed highlighting moving components and motion trajectories ; (d) images from the powder spreading experiment using stainless steel 316L 15 μm–45 μm powder and 250 μm layer height (Permission to reproduce these images was obtained from the authors and the publisher).

A patent application describes a device for evaluating powder spreadability for AM applications [29]. This device includes a powder support surface, a powder dispenser with a hopper, and a spreading system. It spreads a premeasured volume of powder sample, and the spread area is visually inspected to assess spreadability.

Mitterlehner et al. developed a spreading testbed to investigate the influence of powder moisture on its spreadability [30]. Their testbed is a smaller version of commercial PBF machines including a vertically moving feeder, build platform, and overflow bins at each end and a belt-driven moving blade as the spreader. All components are controlled by a LabView program. The surface profile and the existence of empty areas were investigated by removing the builder platform from the testbed and moving it under a digital microscope. Using image analysis techniques, they evaluated the fraction of empty space using maximum height difference and the difference between the third quartile and the first quartile relating to the height distribution of observed particles on the powder layer as the parameters describing the spreadability.

Phuc et al. designed a modular spreading testbed with a powder hopper, feeder module, a recoater module, and spreading platform with manual height and tilt adjustments [31]. They attached a commercially available contact image sensor, used in flatbed scanners, to the recoater mechanism, behind the blade to image the resulting powder layer. The image sensor has an optical resolution

of 5.3 μm/pixel over a length of 210 mm, capable of visualizing individual particles over the entire width of the layer. Due to the narrow depth of field of the sensor, the resulting images have in-focus and out-of-focus zones. Using various image analysis techniques, the uniformity of the powder layer and powder bed defects was assessed.

Chen et al. investigated the mechanisms influencing the powder layer density by computational modeling and experimental validation on commercial PBF equipment (instead of a dedicated powder spreading testbed) [32]. Experimental powder layer density was determined by sintering enclosures on the build platform and weighing each enclosed powder sample offline.

As seen from these latest efforts, the existing testbeds mostly utilize imaging systems to image the spread area and, by image analysis, extract various parameters resulting from the spreading action. None of these testbeds are capable of observing/measuring particle motion during spreading, which is the basis for most computational models.

The primary objective of our PST is to provide direct observation of the powder layer's cross section during the spreading process. The secondary objective is to provide quantitative characterization of the powder layer after spreading. The mechanism of powder flow while spreading can be studied in great detail using particle tracking with the PST. Furthermore, theories such as the existence of the critical velocity of a blade-type spreader can be verified. This will be possible since the particle tracking data obtained from PST experiments is based on cross-sectional view of the powder layer during spreading, enabling the evaluation of mass flow rate. The current configuration of our PST only allows blade-type spreading. Other types of spreaders such as a roller-based spreading mechanism can be implemented in the future to conduct comparative studies. New blades with different shapes (e.g., round profiles or flat profiles) can also be readily integrated with the PST. Other enhancements such as control over spreader vibration or compaction of the powder layer can be implemented in the future. Knowledge and data from PST experiments will be complementary to modeling efforts, allowing modelers to validate and improve their models. Combining these efforts will provide important insight into the physics of powder spreading. The PST is being continuously improved for better performance and to accommodate features required for future experiments. This article describes the design and preliminary results from the first particle tracking experiment on the PST.

2. Powder Spreading Testbed at NIST

The functionality requirements of a spreading testbed can be divided into two categories, the achievement of dynamic properties of the spreading process and the static properties of the spread powder. The primary focus of the PST is on achieving the dynamic properties of the spreading process. The secondary focus of the PST would be to study the properties of spread powder. Further capabilities are planned to be added to the PST according to possible future requirements which are discussed in this section. As previously stated, the current configuration of the PST uses a blade-type recoating process popularly used in several PBF machines. As in a PBF machine, multiple layers of powder can be spread layer by layer using the PST.

2.1. The appearance and dimensions of the PST

The PST has two main parts (a) The main instrument and (b) the linear motion controller (Newport XPS Q8). **Fig. 2** (a) depicts the components of the PST. The recoater arm located above the baseplate is translated along the x-axis by the linear actuator assembly. A secondary linear actuator (Newport LTA HL) attached to the Newport MVN80 vertical stage is used to translate the removable baseplate along the Z-axis. This enables precise control between the baseplate and recoater blade to achieve different powder layer thicknesses. The main instrument is controlled using a wired connection with the linear motion controller.

The Newport XPS controller can be programmed to perform different movements (X-Z) using the remote display or the dedicated laptop and record various output data (position, velocity, accelerations, voltage signals, etc.). This allows movements of the axes, which can be used for spreading powder. The powder heap creation and powder spreading technique will be discussed in detail in section 2.3 and 2.4. For electrical safety, the controller draws power from an uninterruptible power supply (UPS) and supplies power to the main instrument. No additional power supply is required for the PST. The controller can be programmed to execute multiple sequences of movements with the PST and record various output data (position, velocity, accelerations, voltage signals, etc.). A dedicated laptop is connected to the XPS-Q8 controller (**Fig. 2** (a)) using an ethernet cable to send programs and receive output data files. A front view of the PST is also given in **Fig. 2** (b). showing the PST placed beside a high speed camera for experiments.

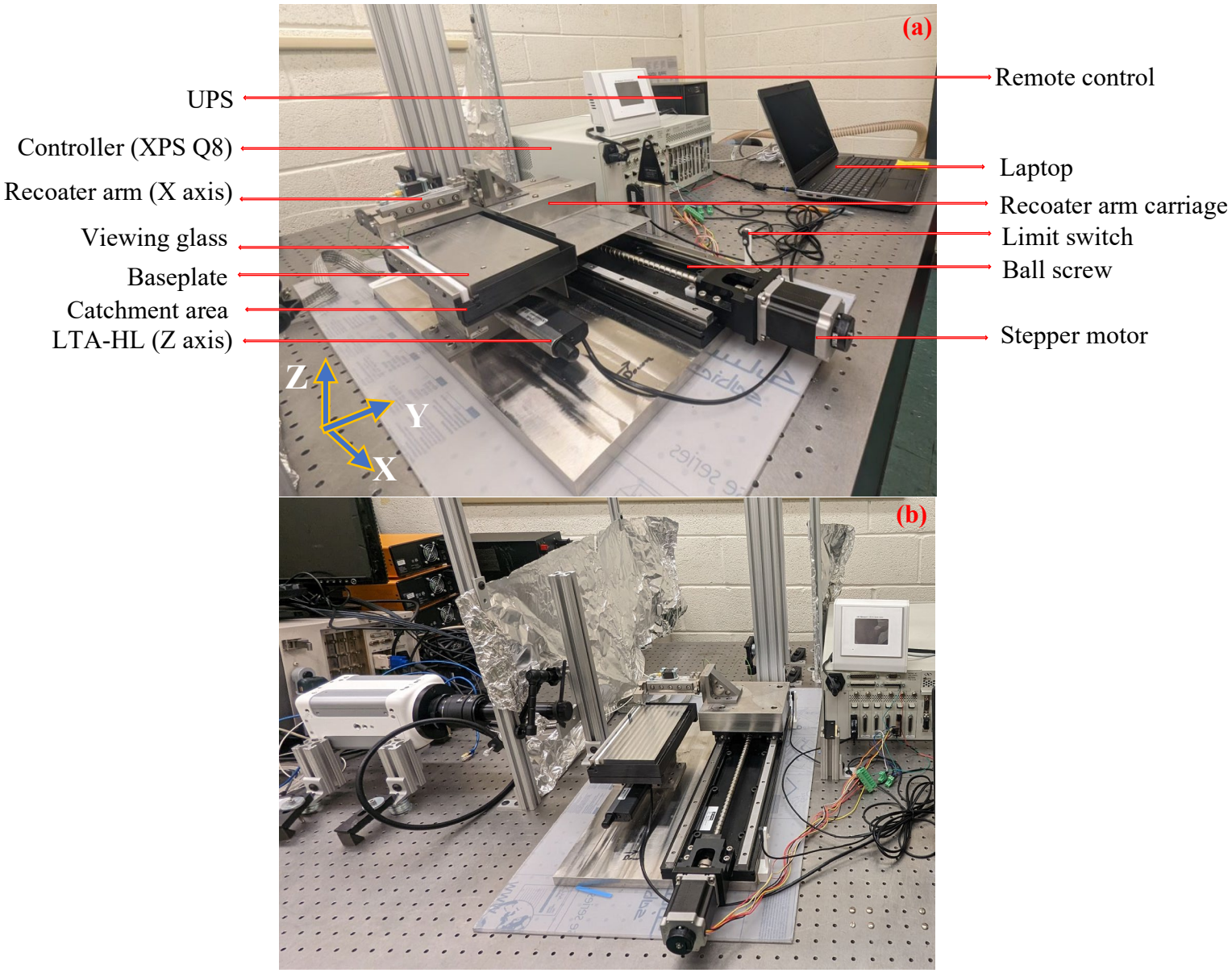

Fig. 2. (a) The PST is viewed from a side including labels for relevant components, the baseplate is seen in front and the XPS Q8 controller is seen at the rear and (b) a front view of the PST.

Further details on the components of the PST labeled in **Fig. 2** (a) are described below:

Recoater arm: The recoater arm or the bridge allows to affix the recoating blade on its front surface or in the powder spreading direction using M4 screws. The recoater is required to be a blade and a ceramic blade is currently being used. The recoater arm is bolted to the movable block (recoater arm carriage) making this the X-axis.

The recoater arm was designed to mount instruments for measurement or modification of the spread powder below. There are 14 tapped M4 screw holes on the upper surface of the recoater bridge to aid this purpose. Currently, any large loads (> 500 g) are intentionally not placed above the bridge purely for ergonomic reasons.

Baseplate: The baseplate is a stainless-steel plate where metal powder is spread by the action of the recoater arm. It has a rectangular top surface of 200 mm x 100 mm and is detachable using four screws to the PST from below. Therefore, it is removable and replaceable using other baseplates with different surface finishes if required. The current configuration of the PST only fixes the baseplate and does not allow any adjustments on tilt in any direction. Once the baseplate is attached an inspection is conducted to confirm the absence of any unwanted tilt.
Catchment area: The catchment area is an area to capture any powder overflow from the baseplate. It prevents any spill caused by the action of the PST. It is a 3D-printed part whose lower end can be detached to dispose of the captured powder.
Controller: A motion controller (Newport XPS Q8) is used for two-axis motion control. It also supplies power for both axes. The controller can accept manual input using the remote control or run programs sent via the attached laptop computer.
Remote control: The controller has a remote control (touchscreen display) that indicates the positions of the stages (both axes). It also allows manual control by offering options to move or jog at each stage.
LTA-HL: It is a linear actuator (Newport LTA-HL) attached to a Newport MVN80 vertical stage which provides precise unidirectional movement to control the height of the baseplate (Z height). Therefore, this is the Z axis of the PST. The movement of the LTA-HL has a bi-directional repeatability of 0.3 μm and has a bi-directional accuracy of 1.2 μm. It is connected to the XPS Q8 controller using a DB 25 connector cable.
Viewing glass: This is an elongated rectangular glass piece that allows powder-spreading imaging or videography from the side. While spreading it is designed to move along with the recoater arm blocking the powder from flowing out of the baseplate from the side.
Recoater arm carriage: The recoater arm carriage supports the recoater arm using an angle bracket. It travels on the linear rails with its travel bounded by the limit switches.
Stepper motor: An Applied Motion HT17-275 stepper motor is used to drive the ball screw using a coupler. The motor is connected to the XPS Q8 controller.
Ball screw/Linear actuator: It is a part of the linear rail (single-axis unit, Misumi KUH1210). This is a ball screw-driven linear slide that accommodates the recoater arm carriage.
Limit switches: There are two contactless sensors at either end of travel that can detect if the recoater arm carriage is close to them. These are induction-based proximity sensors (Panasonic GX series) which are mounted on plastic mounts and connected to the controller's stepper motor input.

The testbed was designed to achieve a balance between being small enough to not require an excessive amount of powder and also mimic a commercial LPBF machine. The baseplate has a length of 200 mm and a width of 100 mm. Commonly, the build platform of a commercial LPBF machine is 250 mm square. This reduction in the length was a concession to achieve the aforementioned balance. The width was significantly reduced based on an assumption that the physics of powder spreading is effectively continuous along the recoater blade after a certain length scale is achieved (e.g., 100x the median particle size). This is not the case for the length (direction of powder spreading), since as powder is spread the initial heap will be depleted. A secondary incentive for maintaining a smaller footprint is the ability to move and place the entire testbed in an environmentally controlled chamber. Additionally, surface analysis, overhead imaging, and other relevant instruments can also be mounted on or affixed near the PST.

Theoretically, it would allow comparison with an LPBF unit. The work conducted by Fox and Whiting will serve as a starting point for characterizing the spread powder layer [9]. A suitable powder sampling technique will be employed in the PST.

2.2. Vibration analysis of the PST

It is understood that during the PBF process, there is potential for undesired recoater motion. This can be caused by a variety of mechanisms, but commonly this is due to impact with solidified AM parts. This impact results in a lifting of the recoater blade while it passes over solidified AM surfaces and is followed by oscillations once the recoater passes the part. This vibration is eventually dampened. As with any other mechanical system, the recoater's dynamic behavior can be characterized. This can be done in-process or post-process. Post-process characterization may include a force-response analysis using a dynamometer and some sort of displacement measurement (e.g., dial gauge, laser triangulation, and interferometry). In-situ characterization may include gyroscopes and accelerometers, which after a double integration can be used to estimate displacement. The recoater could also be instrumented with sensors to directly measure the displacement (as opposed to using accelerometers) and force required to spread the powder.

Vibration analysis of the PST is important. To measure vibrations, a small triaxial accelerometer was mounted on the recoater arm as shown in **Fig. 3** below. The PST was operated without any powder in incremental speeds from 1-20 cm/s. Across most of the speed range, the natural frequency of vibration ranged from 88-390 Hz with amplitudes less than 1 μm RMS. However, there is an additional spectral peak when the slide moves at around 18-19 cm/s. The authors believe this is due to unwanted vibrations from the motor and are in the process of verifying and remedying this. Vibration amplitude was maximum along the X-axis or spreading direction compared to the other axes. The PST possesses a small value of maximum vibration amplitude in comparison with vibration found in commercial equipment [5].

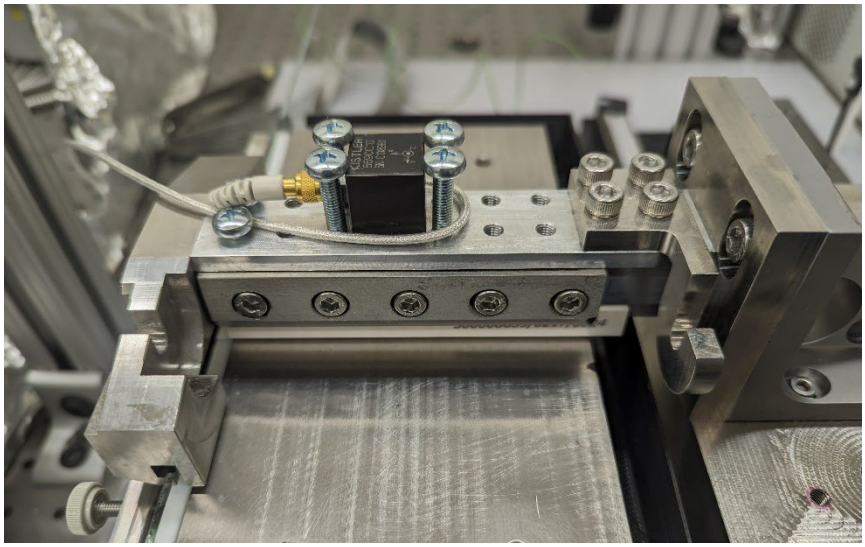

Fig. 3. A triaxial accelerometer is mounted on the recoater bridge to measure vibration.

2.3. Powder heap creation methods

The powder heap is defined as the amount of powder in front of the blade before recoating. This is referred to as the charge in some commercial PBF machines and its initial quantity is often a user-controlled variable. To create the initial powder heap or charge for spreading on the PST, a required amount of powder needs to be poured on the baseplate. To create this heap, two methods, (a) stencil and (b) cylinder-based apparatus are used. The stencil-based mechanism uses a plastic stencil placed on the baseplate where the powder is poured, and the top is scraped with a razor blade as shown in **Fig. 4** (a). Thereafter the stencil is lifted to create a consistent heap as seen in **Fig. 4** (b).

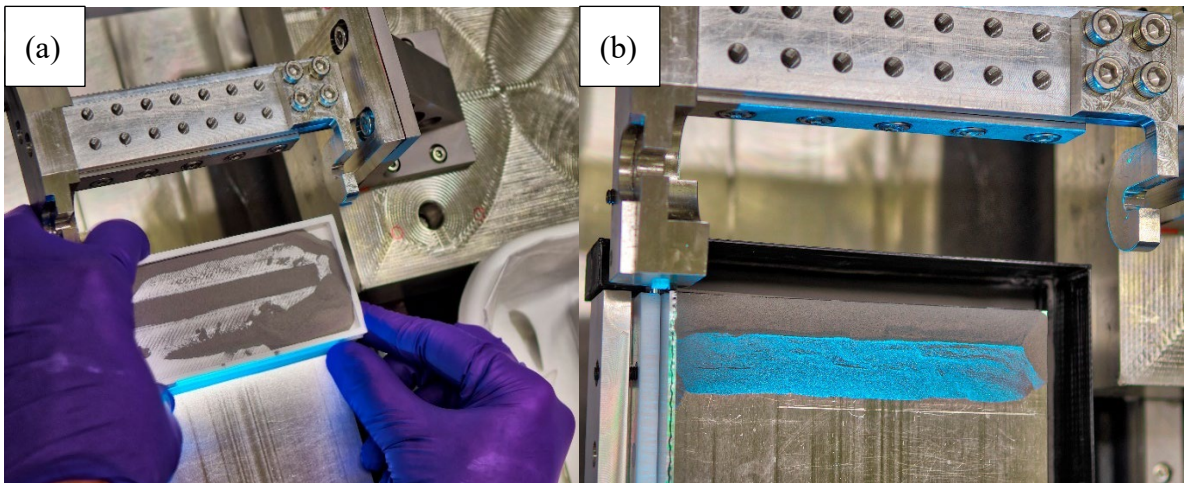

Fig. 4. (a) The plastic stencil placed with powder poured into it and (b) the heap of powder after removing the stencil. The blue light seen in the images are not a part of the PST but results from the handheld camera used for taking the photographs.

The cylinder-based mechanism uses a steel cylinder which is required to be filled with a desired quantity of powder first. Thereafter, it can be lifted and placed on the hooks in front of the recoater arm as shown in **Fig. 5** (a). The cylinder is twisted using the white knob at the end of the cylinder. Thereby, powder pours on the baseplate and creates a heap as seen in **Fig. 5** (b). Both methods were found suitable for spreading powder, with the stencil-based method more convenient for single-layer spreading. The cylinder-based method is well suited for multi-layer spreading since placing the stencil on a spread layer of powder is undesired. Since the cylinder involves the powder falling from a height, the powder heap is more distributed compared to the stencil which produces a narrower heap.

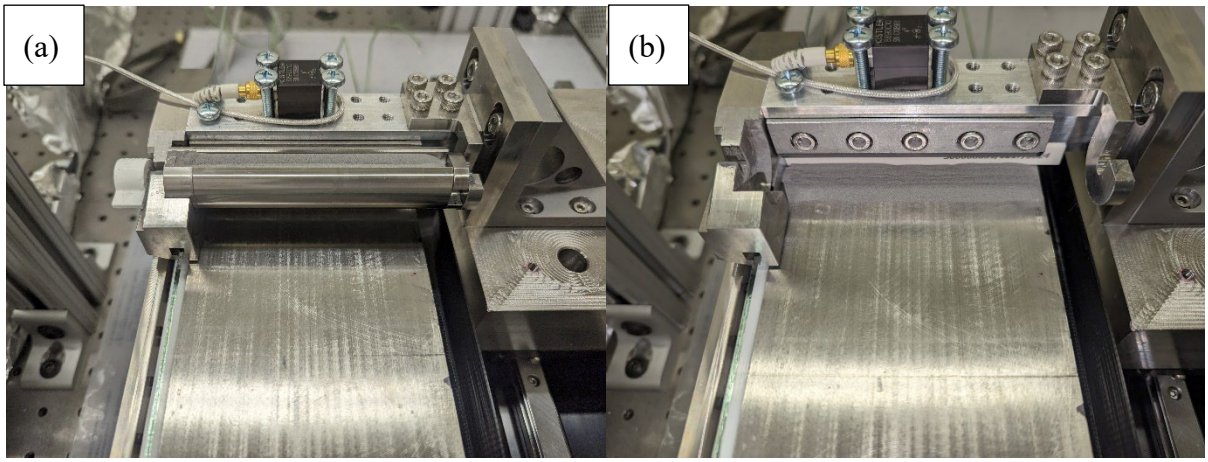

Fig. 5. (a) The cylinder is filled with powder, lifted, and placed on the PST, and (b) the heap of powder is created by turning the cylinder using the white knob at the end.

These two methods of creating the powder heap were chosen for simplicity and size. Some LPBF machines have a powder supply platform that rises allowing the recoater to collect powder into a heap before reaching the build area. Using this method in the PST would have required significantly more space, which was undesirable for reasons previously discussed, and would have required additional motion systems and control. Since a readily created heap is also spreadable, the PST does not involve a powder collection mechanism. The authors acknowledge that the heap creation method may impact some aspects of spreading, e.g., the density of the powder heap in front of the recoater and were willing to trade the fidelity of recreating the heap in the same method as commercial machines to achieve other design requirements.

2.4. Powder spreading method

The ability to spread powder is a critical function for the testbed. Along with this come two further considerations: the ability to conduct multi-layer spreading and the ability to control the layer step height between consecutive layers. Quite often, the focus of powder spreading research is simply placed on single-layer spreading, and more often than not, solely on spreading powder on a smooth surface. However, this only takes place in the actual LPBF process for the first layer. The vast majority of the spreading process in an actual LPBF build takes place over either loose, previously spread powder or over previously solidified surfaces. The PST is designed in a manner to allow both single and multi-layer spreading to be comparable to LPBF spreading processes. Furthermore, if needed future plans may involve adding a roller or even non-contact spreading processes enabling the PST to be a comprehensive testbed.

As discussed previously in section 2.1, the position, speed, and acceleration of both axes (X: Recoater and Z: Z-stage/baseplate) are controlled using the XPS Q8 controller. The inputs, limits, and behavior of the motor are controllable via a .ini settings file accessible within the controller. The velocity profile for the X axis is an S gamma curve, indicating that the motor is accelerated to the target velocity, held at constant velocity, and then decelerated to zero velocity. This type of profile is ideal for the PST since constant velocity is desired during spreading. The

maximum allowable velocity is set to 200 mm/s as it is sufficient to replicate practical powder spreading processes and also prevent undesirably high speeds on the PST [33]. It was observed with the PST's current setup that an acceleration higher than 40 mm/s^2 was producing unwanted noise from the stepper motor during operation. Therefore the acceleration value is set to 40 mm/s^2.

The inputs, limits, and behavior of the LTA-HL (Z-axis stage) can also be controlled via a .ini file (using standard values since it is from the same manufacturer as the controller) accessible with the controller. Precise control over velocity or acceleration is possible but not necessary for the Z axis since it is static while the powder is spreading. The position feedback is important and available via encoder feedback from the instrument. The position feedback can also be read from the remote display or via the controller's local web interface if connected to a computer. Both stages can be controlled manually after disabling them using the controller. This is particularly important for the Z axis since positional feedback is available on the remote control display via the encoder output. Therefore, the Z height can be adjusted by disabling the axis and manually adjusting the black knob on the LTA HL and the position can be seen on the remote control display. Since the Z height requires setting whenever the recoater blades or layer heights are changed or verified, the homing method is set to retain its current position for ease of use.

2.5. Cross-sectional imaging for particle tracking

During the spreading process, many individual particles contact other particles as well as the recoater blade and the substrate. The aggregate of these interactions determines the powder's bulk behavior to the applied stress. The PST allows the evaluation of the particle-particle, particle-recoater, and particle-substrate interactions. Data collected can be used to directly validate and calibrate modeling efforts. Particle tracking is one of the tools to investigate the aforementioned dynamic properties of the spreading process. A Photron Fastcam Nova S16 high-speed camera and a telecentric lens were set up on the optical bench for this purpose [34, 35]. The camera lens is perpendicular to the spreading direction. This allows the spreading process to be imaged through the glass as shown in **Fig. 6**. The aluminum foil held by aluminum bars is a temporary measure to protect from any stray powder and disturbance from any blown air from the controller, uninterruptible power supply (UPS), or computers. The maximum bit rate (bytes per second data can be transferred from the camera sensor to the camera's internal memory) of this high-speed camera is 2 GB/s. This translates to about 5.46 s of video capture at 1024*1024 pixel resolution at 16,000 frames per second (fps) to fill up a 128 GB dedicated memory. There are 4096 intensity levels (12 bits) per pixel. Either frame rate or frame resolution can be lowered to allow longer video capture.

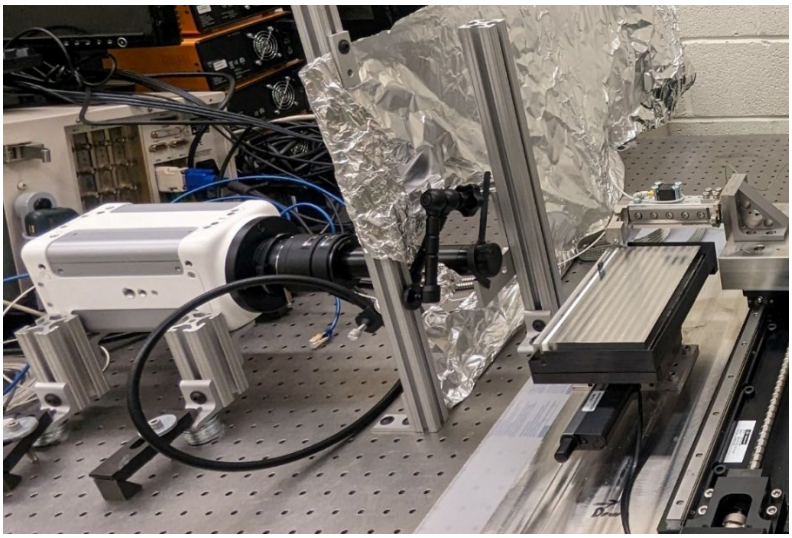

Fig. 6. The Photron NOVA high-speed camera positioned to look into the PST for videography.

The lighting is provided by a Prizmatix UHP-F-5-625 ultra high power red light emitting diode (LED) and a Prizmatix LLG-5 liquid light guide. We have several lenses to choose from, but the two most commonly used lenses for this testbed are the Myutron FTV60C-110 6x telecentric lens and the Myutron FTV40-110 4x telecentric lens. These can be used as is or combined with either a Kenko TELEPLUS HD pro 1.4x DGX Teleconverter or a Kenko TELEPLUS HD pro 2x DGX Teleconverter. While telecentric zoom lenses are available, this often results in slightly different magnifications from test to test. Since the arrangement uses fixed components that have no moving parts, calibrated values should stay more constant from test to test. As shown in **Table 2**, using two lenses and two teleconverters, six magnifications can be achieved.

Table 2. Magnifications achievable with the commonly used lens systems.

Lens	Teleconverter	Scaling (px/mm)	Max. Field of View (mm)
4x	None	263	3.90
4x	1.4x	369	2.78
4x	2.0x	530	1.93
6x	None	394	2.60
6x	1.4x	553	1.85
6x	2.0x	794	1.29

Fig. 7 shows one captured instance of powder spreading using the 4x lens and the 1.4x teleconverter. The recoating speed was 60 mm/s, with a 50 μm layer height on top of existing layers of powder. The recoater blade pushes a heap to spread the powder. As seen in the figure, some particles have escaped within a small gap between the recoater blade and the glass. The PST will be improved in the future to mitigate this issue. The powder heap in case of multilayer

spreading does not include the leftover powder from the previous pass(es). Powder underneath the blade will be called deposited or spread powder. It is noted that the exact location of the interface of these two regions is currently unknown and likely variable, dependent on the conditions of spreading (e.g., recoating speed, recoater blade material, environmental conditions, and powder properties). Though these details are of great interest, how and where the heap is sheared is an important contribution to a full characterization of the powder spreading process. The powder that is spread or deposited on the build substrate is separated from the heap at some junction. How it is separated (i.e., shear plane characteristics) will dictate the spreading performance. These can be visualized via particle tracking by processing the videos collected using a high-speed camera. Since particle tracking provides processed results, details from one set of experiments are provided in Section 3.

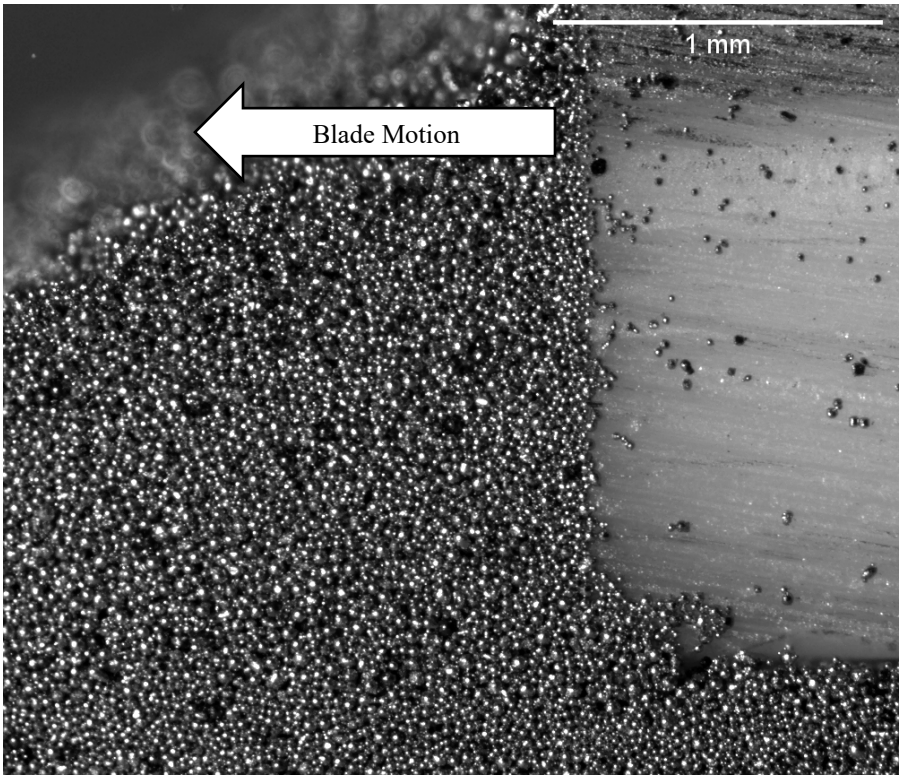

Fig. 7. Still image of recoater blade spreading stainless steel powder captured using the high-speed camera set up. The field of view measures 2.71 mm x 2.33 mm.

While it is likely that a large portion of the heap moves as a unified mass, there will be regions or interfaces of shear. The particular nature of these shear planes dictates how a powder is spread and is therefore closely related to the characteristics of the spread powder (i.e., height, density, and PSD). The nature of these shear planes has not yet been fully characterized.

3. An initial result and a brief methodology of particle tracking

The results from one initial particle tracking effort while spreading coarse stainless steel powder feedstock (D50=38.4 µm) with recoater velocity at 60 mm/s are documented in this section. Additionally, the layer height has been set to 40 µm and this spread is conducted over previously spread powder (multi-layer spreading) as possible in LPBF equipment. As described in section 2.4, the high-speed camera can be positioned to have a field of view that contains the baseplate and the moving heap of powder in front of the recoater blade. Therefore it captures information regarding particle flow in front of the recoater blade during powder spreading. Three such snapshots of particle flow in front of the recoater blade are presented in **Fig. 8**. The frame rate of the video is 16 000 fps, and the resolution of each frame is 1000 pixels by 860 pixels. The field of view measures 2.71 mm x 2.33 mm and the scaling is 2.71 µm/pixel. Data from all 1851 frames of the video were subsequently combined to create a composite view. The total length of time of the video is only 116 ms. If one assumes that how the powder flows is relatively time-invariant during this narrow window of time, the resulting composite view may be seen as a reasonably accurate representation of how the powder particles flowed during that specific time interval. This allows researchers to follow their motion as they are pushed by the recoater blade. Readers are encouraged to view the high-speed video of powder spreading via the link provided in the appendix section. The playback speed is 30 fps, so it plays 533 times slower than the actual spreading.

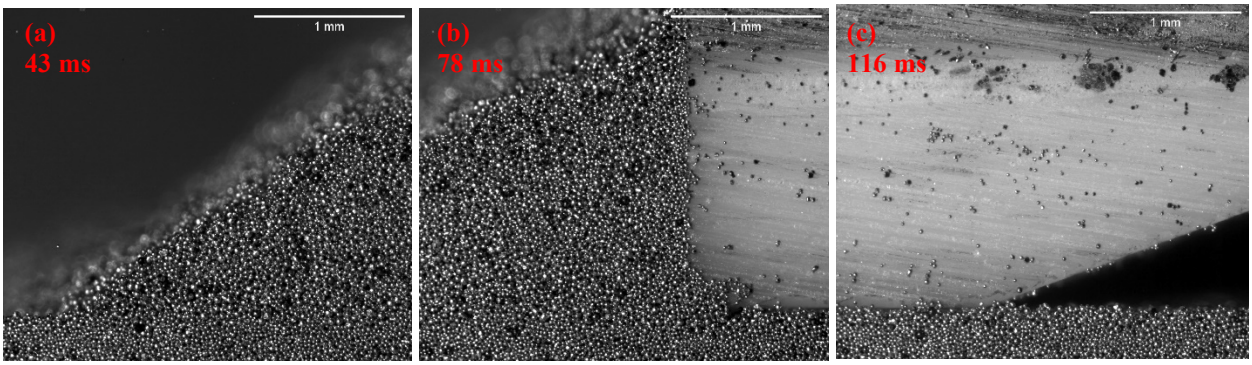

Fig. 8. Still imagery extracted from high-speed videography (total 116 ms long) of powder spreading: (a) heap advancing before spreading (after 43 ms), (b) during spreading (after 78 ms), and (c) after the front of the blade has passed (after 116 ms). The field of view measures 2.71 mm x 2.33 mm and the scaling is 2.71 µm/pixel.

Particle tracks were calculated from the video through image processing. The details of how this is accomplished will be given in a companion publication currently under preparation as of October 2023 [36]. A summary of particle tracking will be provided in this section. The tracking software determines the raw track data from the video [36]. Mathematically, a particle track is a list of triples (Frame Number, X Location, Y Location). There is one triple for each frame in which that particle was found. Since the video was acquired at a constant frame rate, the frame number is equivalent to a time stamp. With both time and location being known, parameters such as velocity and acceleration can be computed from the track data.

The next step is to manually mark the blade location in the video. The blade velocity is then estimated by the software and verified against experimental settings. Initially, all track locations

are relative to the stationary camera. However, when the blade location and velocity are known, the locations of the tracks may be adjusted so that all locations are relative to the blade. A plot of the tracks is shown in **Fig. 9**. Each track is assigned a random color to make it easier to differentiate one track from another. The outline of the blade is shown in black.

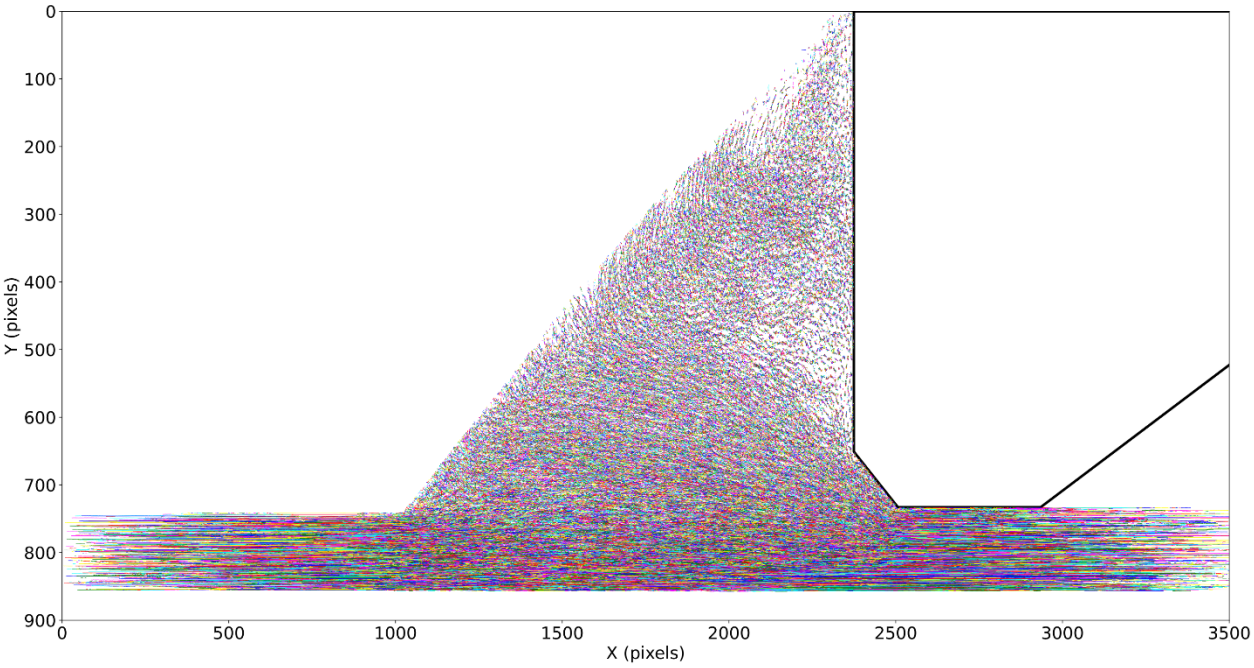

Fig. 9. Plot of particle track data using random colors.

In addition, one can employ vector fields for flow characterization, as is often done in particle image velocimetry (PIV). This can be determined from the track data in many ways, but two similar ways are shown in **Fig. 10** and **Fig. 11**. To create the vector fields, a user-specified, uniformly spaced grid is placed over the track data. At each node of the grid, a "typical" behavior of all the tracks in that local neighborhood is represented by a vector centered on that node. Note that there are many ways to define what is typical behavior. A weighted average of the local track velocities was used here. Velocity relative to the stationary camera is shown in **Fig. 10** and velocity relative to the moving blade is shown in **Fig. 11**. The direction of each vector represents the typical direction of the tracks in that neighborhood. The color of the plot around the vectors indicates the magnitude of relative velocity. Tracks and vector fields each have advantages and disadvantages, which are discussed in the companion publication [36].

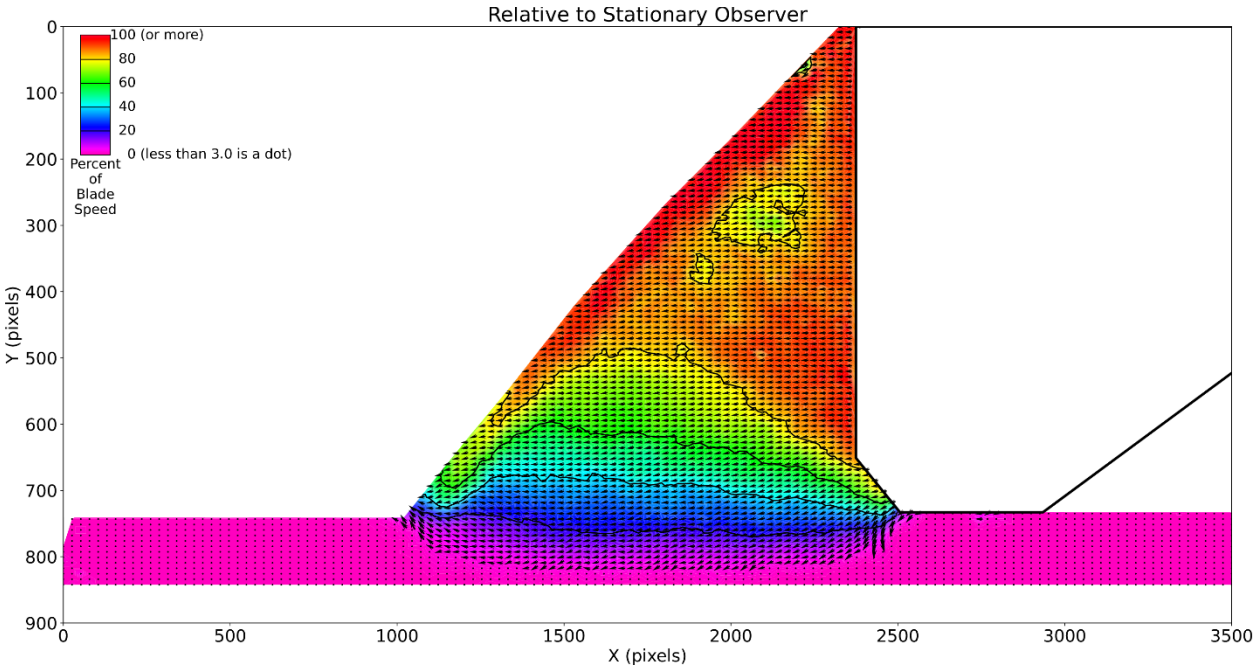

Fig. 10. Plot of the vector field with colors indicating velocity relative to the stationary camera. Since the baseplate of the PST is also stationary, this plot is especially informative near the baseplate, since it may indicate what frictional forces are likely between the particles and the baseplate.

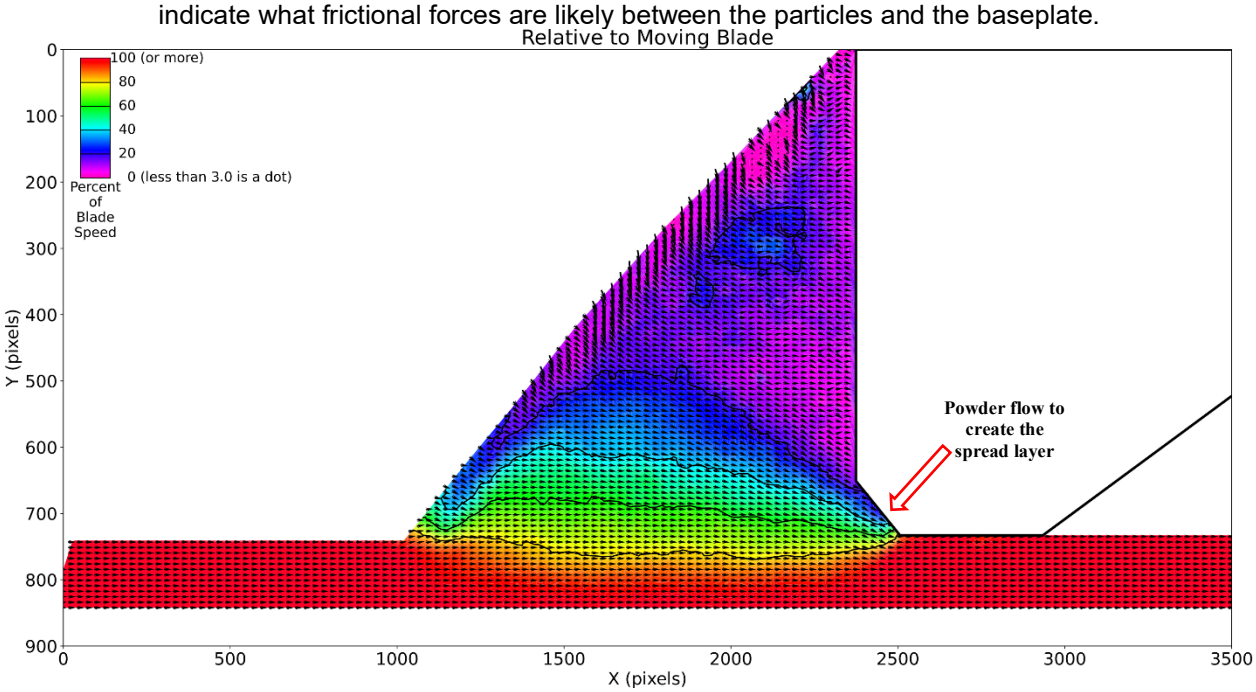

Fig. 11. Plot of the vector field with colors indicating velocity relative to the blade. This plot is especially informative near the blade, since it may indicate what frictional forces are likely between the particles and the blade.

In this case, the fastest flow response occurs several layers above the spread layer and also along the recoater blade wall and the heap incline seen by the red zone in **Fig. 10**. Furthermore, looking at **Fig. 11**, it is observed that as the recoater blade pushes the heap, powder flow occurs between the gap between the spread powder and the blade. Therefore the vectors near the small front incline of the blade indicate a stream of powder flowing into this gap as marked by the red arrow

in **Fig. 11**. This is the powder stream which either recoats the bed or is pushed down into the previous powder layers. Above the small incline of the recoater blade shows comparatively slow powder flow. Also as evidenced by **Fig. 9**, starting from the incline the powder flow follows an arc-like path from the heap indicating a pull response of powder affected by the flow of powder near the blade. Finally, in **Fig. 11** it can also be observed that the moving heap scrapes up particles from the spread powder as evidenced by the vectors in front of the moving heap.

The analysis provides useful insight into the fundamental mechanisms of powder flow in front of the recoating blade. Therefore it is possible to divide the heap into its corresponding flow zone as theoretically conducted by Zhang et al. using DEM simulations on polymeric powder [22]. However, such characterization in the case presented in this paper would require the data to be captured at different relevant spreading velocities to verify the consistency of the zones. This is one of the future works planned to be conducted using particle tracking with the PST.

4. Characterization of spread powder layer

Characterization of the spread powder layer includes the post-analysis of spread powder to evaluate PSD, powder bed density, and spread height. A high-quality spread powder bed should not possess streaks, unevenness, gaps, or other undesired features that can translate to defects in LPBF parts [37]. Unfortunately, a single metric for determining the surface condition or quality does not exist for a spread powder. Therefore a host of characteristics are employed to understand the quality of the surface. Information from one might be interrelated with the other parameter but all of them provide unique information on the spread layer. The surface PSD allows to check any deviation from the bulk PSD. The density of the powder bed focuses on attaining a certain level of packing or powder bed density for feasible builds with the LPBF process. In a set of density measurements, a lower value might indicate improper packing and chances of voids or cracks in the built part. Height measurement serves two major purposes, (a) before spreading powder the flatness of the baseplate can be ensured and (b) post-spreading a height map of the surface is desired to check any unwanted features on the surface.

4.1. Particle Size Distribution (PSD)

In the usage of the PST, the aim would be to spread single or multiple layers of powder. A simple sampling technique, dubbed the ‘cookie cutter method’ will be used. It uses a thin-walled cylinder or cuboid to separate regions of powder. The profile, usually made from metal for rigidity and durability, is plunged axially into the loose powder. It has a thin wall and often a sharpened leading edge to precisely separate the regions. Once the profile is pushed down far enough so that the leading edge is in contact with the substrate, the surrounding powder can be mechanically removed using a brush or other tools. The powder inside the profile can then be collected via a clean brush for the PSD analysis.

A variety of characterization techniques can be used including sizing and morphological characterization. For example, scanning electron microscopy (SEM), dynamic image analysis

(DIA), and laser light scattering (LLS) for size measurements. Furthermore, captured powder can be subject to chemical analysis using inductively coupled plasma optical emission spectrometry (ICP OES).

4.2. Spread layer height

The height of the spread layer can be evaluated in various ways on the powder spreading testbed. Among these, two techniques and preliminary results will be discussed as follows,

1. View from the side: Lateral imaging using an aligned camera provides a view of the thickness of the spread layer. The length calibration for this camera was conducted independently with a tri-bar air force target and other test targets. Images can be taken during or after powder spreading to obtain the distribution of the powder against the viewing glass as demonstrated previously in section 2.4.

2. Measurements using an optical point scanner: A laser triangulation-based point scanner (Keyence LKG32) was aligned by laying it flat on the baseplate and thereafter affixed on top of the recoater arm as shown in **. Fig. 12** (a). It uses a 655 nm (visible light) laser with a 30 micron diameter circular spot size. The measurement range is ± 5 mm for diffused reflection and it has a repeatability of 0.05 micron. The instrument was tested to resolve artifacts and height changes of 1 micron. The sensor has its output connected to the XPS Q8 controller for data acquisition. As the recoater arm moves, the sensor is capable to perform a linear scan. In this way, height data can be collected over one line of the spread powder layer. One such set of sample data was collected over spread stainless steel powder with a layer thickness < 100 µm as shown in **Fig. 12.** (b). It shows the distribution of the height over a two-dimensional profile with the flat portion of the data indicating the bare baseplate. The scan was started from a point in the bare base plate (referenced as 0 in the X axis) beyond the end of the baseplate and the measurement scan was repeated. Therefore, the initial portion up to around 20 mm in the X axis in the graph presented in **Fig. 12.** (b) shows the tilt of the baseplate thereafter transiting to higher values of data due to the spread powder. Expectedly, beyond the baseplate (around 170 mm of travel) the signal drops abruptly. One portion of this graph (from 50-51 mm) depicting the profile of the spread layer has been zoomed in and plotted as **Fig. 12.** (c). The features of the individual powder particles cannot be seen but an averaged pattern was found. Although this method cannot provide the height data over the entire spread, it does allow to have one estimate of the spread powder height and major variations. Importantly this method has allowed us to detect any baseplate tilt and its direction quickly without using manual indicators. It was found that any extant baseplate tilt could be easily adjusted post point scanning.

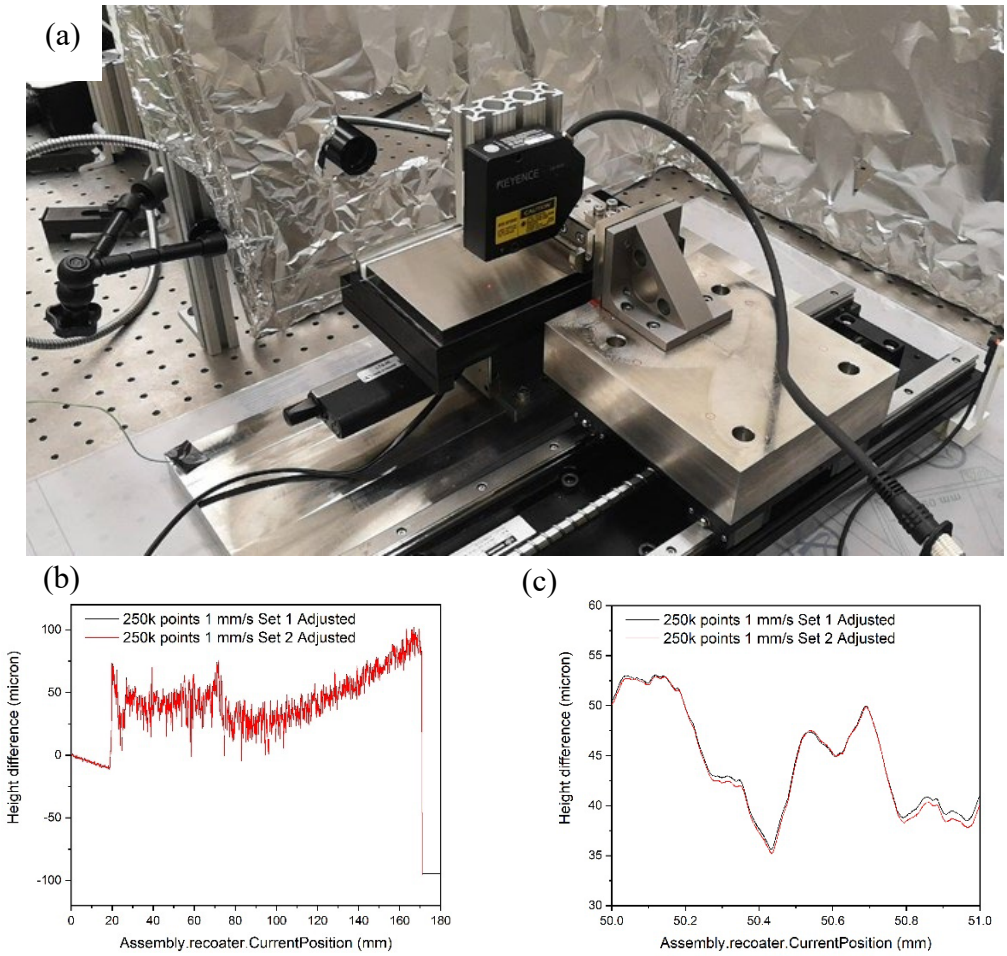

Fig. 12. (a) Image showing the LK G32 laser point scanner attached to the recoater arm of the PST, the black lens of the Photron NOVA high speed video camera is visible in the background, (b) plot of height data over the entire span of spread powder (set 2 indicates the second scan) and (c) zoomed-in view of height data at 50-51 mm of the same powder spread.

The spread height analysis is a work in progress that ultimately aims to provide three-dimensional characteristics of the spread powder layer including the overall profile and flatness of the spread.

4.3. Powder layer density

Quantifying the density of the loose powder is not always straightforward, particularly so, when attempting to characterize it in an in-situ manner. A granular media in a static state is easily disturbed. Clearly, a well-known volume of powder must be defined, which will then be used, along with its mass, to calculate the sample's density. A "cookie cutter" type separation as discussed in section 4.1 with a well-known area can be used to separate a region of powder. This area along with the powders' height provides the volume. The height can either be measured, or one can use the vertical distance between the underside of the recoater and the substrate the powder was spread upon. The final step is simply extracting this region of powder and weighing the sample.

5. Environmental chamber

Moisture can play a significant role in the dynamic behavior of granular materials [38]. Directly measuring moisture content in metal powders is not straightforward. Some techniques may be used to analyze small samples for moisture content, but this requires sampling the powder and loading it into another device. Depending on the sorption and desorption rate of the granular material, this removal process may alter the moisture content. Preliminary work has shown while sorption testing is plausible with AM metal powders, thermogravimetric analysis (TGA) is not sensitive enough [37]. TGA allows the moisture content to be directly measured by encouraging vaporization using thermal energy and simultaneously weighing the sample. Even when the powder was subjected to high levels of moisture (i.e., 80% relative humidity) for more than 24 hours, no detectable levels of water were found. On the other hand, sorption testing does not directly measure the moisture content of a sample, but rather the water sorption and desorption rates by subjecting the sample to constant relative humidity levels for periods and then weighing the sample. While this allows one to categorize certain materials for their ability to adsorb and desorb water, it will not allow for a comparison of the moisture content of samples. Because of these findings, while it is suggested that a spreading testbed be able to control the environmental conditions, providing a means to measure the powder's moisture content is not recommended.

Most PBF processes are conducted inside chambers filled with inert gas (i.e., argon or nitrogen) to avoid oxidization and other undesirable chemical reactions. A spreading testbed should be able to closely replicate the environmental conditions present in the actual PBF process. During the next design, a means to do so shall be considered. Either a chamber with pass-through cables for power and data transfer should be constructed or if the entire footprint is kept small enough, the system can be placed in an existing environmental chamber.

6. Conclusion

A powder-spreading testbed with the ability to *in-situ* image the cross-section of the powder-spreading process has been developed. Results from a particle tracking experiment while spreading stainless steel powder were provided. This serves as a reference to the current capabilities and the immediate future projects with the PST. Aside from this imaging technique, a sampling method will be implemented so that powder bed densities and particle size distributions can be calculated for single and multiple spread layers. Finally, it is recommended that the recoater arm be instrumented with sensors that provide data regarding the recoater's dynamics. Examples presented include the accelerometer and the point scanner which was mounted on the recoater. These three capabilities will provide robust data sets with the ability to characterize the spread powder as well as the physics of the actual spreading process.

References

[1] Hu Z, Gao S, Zhang L, Shen X, Seet HL, Nai SML, Wei J (2022) Micro laser powder bed fusion of stainless steel 316L: Cellular structure, grain characteristics, and mechanical properties. *Materials Science and Engineering: A* 848:143345. https://doi.org/10.1016/j.msea.2022.143345

[2] Powder Motion Labs (2017). Available at http://www.powdermotionlabs.com/leveler/index.html (Accessed 15th November 2023)

[3] Buller B, Milshtein E, Brezpczky TB, Seelinger S (2018) Material-fall three-dimensional printing. Available at https://patents.google.com/patent/US20180133956A1 (Accessed 15th November 2023)

[4] Tang M, Guo Y, Zhang W, Ma H, Yang L, Wei W, Wang L, Fan S, Zhang Q (2023) On recoated powder quality with a forward rotating flexible roller in laser powder bed fusion of 30 wt % 5 μm SiCp/AlSi10Mg composites. *Materials & Design* 225:111489. https://doi.org/10.1016/j.matdes.2022.111489

[5] Nasato DS, Briesen H, Pöschel T (2021) Influence of vibrating recoating mechanism for the deposition of powders in additive manufacturing: Discrete element simulations of polyamide 12. *Additive Manufacturing* 48:102248. https://doi.org/10.1016/j.addma.2021.102248

[6] Dadbakhsh S, Hao L, Sewell N (2012) Effect of selective laser melting layout on the quality of stainless steel parts. *Rapid Prototyping Journal* 18(3):241–249. https://doi.org/10.1108/13552541211218216

[7] Brown CU, Jacob G, Stoudt M, Moylan S, Slotwinski J, Donmez A (2016) Interlaboratory Study for Nickel Alloy 625 Made by Laser Powder Bed Fusion to Quantify Mechanical Property Variability. *Journal of Materials Engineering and Performance* 25(8):3390–3397. https://doi.org/10.1007/s11665-016-2169-2

[8] Slotwinski J, Garboczi E, Stutzman P, Ferraris C, Watson S, Peltz M (2014) Characterization of Metal Powders Used for Additive Manufacturing. *Journal of Research of the National Institute of Standards and Technology* 119:460–493. https://doi.org/10.6028/jres.119.018

[9] Whiting J, Fox J (2016) Characterization of feedstock in the powder bed fusion process: sources of variation in particle size distribution and the factors that influence them. *International Solid Freeform Fabrication Symposium*, *University of Texas at Austin* Available at https://repositories.lib.utexas.edu/server/api/core/bitstreams/d55943cb-27be-43aa-a9ed-975481ae13ee/content (Accessed 16th November 2023)

[10] Sandler N, Reiche K, Heinämäki J, Yliruusi J (2010) Effect of Moisture on Powder Flow Properties of Theophylline. *Pharmaceutics* 2(3):275–290. https://doi.org/10.3390/pharmaceutics2030275

[11] ISO/ASTM 52907 (2019) Additive manufacturing — Feedstock materials — Methods to characterize metal powders. ISO. Available at https://www.iso.org/standard/73565.html (Accessed 16th November 2023)

[12] Seyda V, Herzog D, Emmelmann C (2017) Relationship between powder characteristics and part properties in laser beam melting of Ti–6Al–4V, and implications on quality. *Journal of Laser Applications* 29(2):022311. https://doi.org/10.2351/1.4983240

[13] ASTM B213-20 (2020) Standard Test Methods for Flow Rate of Metal Powders Using the Hall Flowmeter Funnel. ASTM International. Available at https://www.astm.org/b0213-17.html (Accessed 16th November 2023)

[14] ASTM B527-22 (2022) Standard Test Method for Tap Density of Metal Powders and Compounds. ASTM International. Available at https://www.astm.org/b0527-22.html (Accessed 16th November 2023)

[15] Spierings AB, Voegtlin M, Bauer T, Wegener K (2016) Powder flowability characterisation methodology for powder-bed-based metal additive manufacturing. *Progress in Additive Manufacturing* 1(1):9–20. https://doi.org/10.1007/s40964-015-0001-4

[16] Kaye BH (1997) *Powder Mixing (Vol. 10.)* (Springer Science & Business Media, Germany). Available at https://link.springer.com/book/9780412403408 (Accessed 16th November 2023)

[17] Hare C, Zafar U, Ghadiri M, Freeman T, Clayton J, Murtagh MJ (2015) Analysis of the dynamics of the FT4 powder rheometer. *Powder Technology* 285:123–127. https://doi.org/10.1016/j.powtec.2015.04.039

[18] Freeman R (2007) Measuring the flow properties of consolidated, conditioned and aerated powders — A comparative study using a powder rheometer and a rotational shear cell. *Powder Technology* 174(1):25–33. https://doi.org/10.1016/j.powtec.2006.10.016

[19] Beakawi Al-Hashemi HM, Baghabra Al-Amoudi OS (2018) A review on the angle of repose of granular materials. *Powder Technology* 330:397–417. https://doi.org/10.1016/j.powtec.2018.02.003

[20] Yablokova G, Speirs M, Van Humbeeck J, Kruth J-P, Schrooten J, Cloots R, Boschini F, Lumay G, Luyten J (2015) Rheological behavior of β-Ti and NiTi powders produced by atomization for SLM production of open porous orthopedic implants. *Powder Technology* 283:199–209. https://doi.org/10.1016/j.powtec.2015.05.015

[21] Yao D, An X, Fu H, Zhang H, Yang X, Zou Q, Dong K (2021) Dynamic investigation on the powder spreading during selective laser melting additive manufacturing. *Additive Manufacturing* 37:101707. https://doi.org/10.1016/j.addma.2020.101707

[22] Zhang J, Tan Y, Xiao X, Jiang S (2022) Comparison of roller-spreading and blade-spreading processes in powder-bed additive manufacturing by DEM simulations. *Particuology* 66:48–58. https://doi.org/10.1016/j.partic.2021.07.005

[23] Haeri S, Wang Y, Ghita O, Sun J (2017) Discrete element simulation and experimental study of powder spreading process in additive manufacturing. *Powder Technology* 306:45–54. https://doi.org/10.1016/j.powtec.2016.11.002

[24] Wang L, Yu A, Li E, Shen H, Zhou Z (2021) Effects of spreader geometry on powder spreading process in powder bed additive manufacturing. *Powder Technology* 384:211–222. https://doi.org/10.1016/j.powtec.2021.02.022

[25] Ganesan VV, Amerinatanzi A, Jain A (2022) Discrete Element Modeling (DEM) simulations of powder bed densification using horizontal compactors in metal additive manufacturing. *Powder Technology* 405:117557. https://doi.org/10.1016/j.powtec.2022.117557

[26] Nan W, Ghadiri M (2019) Numerical simulation of powder flow during spreading in additive manufacturing. *Powder Technology* 342:801–807. https://doi.org/10.1016/j.powtec.2018.10.056

[27] Hulme CN, Mellin P, Marchetti L, Hari V, Uhlirsch M, Strandh E, Saeidi K, Dubiez-Le Goff S, Saleem S, Pettersson V, Memarpour A, Jakobsson K, Meurling F (2022) A practicable and reliable test for metal powder spreadability: development of test and analysis technique. *Progress in Additive Manufacturing*. https://doi.org/10.1007/s40964-022-00341-3

[28] Oropeza D, Roberts R, Hart AJ (2021) A modular testbed for mechanized spreading of powder layers for additive manufacturing. *Review of Scientific Instruments* 92(1):015114. https://doi.org/10.1063/5.0031191

[29] Godfrey DG, Baughman BG, McNair M, Lastre HA, Guthrie D, Schnepf J, Kielbus R, Dolan J, Harms E, Figueroa M (2020) Devices and methods for evaluating the spreadability of powders utilized in additive manufacturing. Available at https://patents.google.com/patent/US10620103/en

[30] Mitterlehner M, Danninger H, Gierl–Mayer C, Frank J, Tomischko W, Gschiel H (2022) Novel testing device and routine to characterise the spreadability of powders for powder bed fusion processes – a problem-oriented approach. *Powder Metallurgy* 65(4):318–334. https://doi.org/10.1080/00325899.2021.2023414

[31] Tan Phuc L and Seita M (2019) A high-resolution and large field-of-view scanner for in-line characterization of powder bed defects during additive manufacturing. *Materials & Design* 164:107562. https://doi.org/10.1016/j.matdes.2018.107562

[32] Chen H, Wei Q, Zhang Y, Chen F, Shi Y, Yan W (2019) Powder-spreading mechanisms in powder-bed-based additive manufacturing: Experiments and computational modeling. *Acta Materialia* 179:158–171. https://doi.org/10.1016/j.actamat.2019.08.030

[33] Yuasa K, Tagami M, Yonehara M, Ikeshoji T-T, Takeshita K, Aoki H, Kyogoku H (2021) Influences of powder characteristics and recoating conditions on surface morphology of powder bed in metal additive manufacturing. *The International Journal of Advanced Manufacturing Technology* 115(11–12):3919–3932. https://doi.org/10.1007/s00170-021-07359-x

[34] FASTCAM NOVA S-SERIES, Photron (2023) Available at https://photron.com/fastcam-nova-s/ (Accessed 15th November 2023)

[35] The Advantages of Telecentricity, Edmund Optics (2023) Available at https://www.edmundoptics.com/knowledge-center/application-notes/imaging/advantages-of-telecentricity/ (Accessed 15th November 2023)

[36] Whitenton E, Whiting J, Donmez A, Das A, Tondare V, Fox J, McGlauflin M, Moylan S (2023) Implementation of a Particle Tracking Method to Study Particle Spreading in Powder Bed Fusion Systems. *Manuscript in preparation, Engineering Laboratory, NIST Gaithersburg*.

[37] Escano LI, Parab ND, Xiong L, Guo Q, Zhao C, Fezzaa K, Everhart W, Sun T, Chen L (2018) Revealing particle-scale powder spreading dynamics in powder-bed-based additive manufacturing process by high-speed x-ray imaging. *Scientific Reports* 8(1):15079. https://doi.org/10.1038/s41598-018-33376-0

[38] Parker BS (2021) Blending of powders for in-situ alloying of Ti-6Al-4V laser powder bed fusion. Thesis. (Stellenbosch University, South Africa). Available at https://scholar.sun.ac.za/handle/10019.1/110122 (Accessed 16th November 2023)

Appendix

The video for powder spreading described in the results section (Section 3) is available at this webpage https://www.nist.gov/video/high-speed-video-metal-powder-spreading-using-powder-spreading-testbed-pst-nist-0 (Accessed 16th November 2023)